Robotic Air Pluviation for Large-Scale Sand Specimens

Carlos Peña Pinto[1*], *Faith* Abimaje[1], *Luis* Mugele[1], and *Hans* Stutz[1]

[1]Institute of Soil Mechanics and Rock Mechanics (IBF), Karlsruhe Institute of Technology (KIT), Engler-Bunte-Ring 14, 76131 Karlsruhe, Germany

Abstract. Robotic automated specimen preparation (RASP) by single-nozzle air pluviation was originally developed for conventional laboratory specimens with diameters of approximately 100 mm. The present study investigates its transfer to larger cylindrical sand specimens intended for large-scale triaxial and oedometer testing while maintaining reproducible preparation conditions. During this scale-up, however, a center high deposition surface developed and then part of the experimental program aimed to examine its formation and to identify a suitable method for reducing it. For this purpose, washed Karlsruhe Sand (KS) was pluviated into a single ring cylindrical mold with a nominal internal diameter D = 469 mm. The path diameter D_p and path topology (serpentine or concentric) were varied, whereas other influencing parameters, including the nozzle diameter and fall height, were kept constant. The results show that changing the path topology alone was insufficient to eliminate the central crown, as the concentric path still produced a center high surface. By contrast, extending the serpentine path beyond the mold internal diameter to $D_p/D \approx 1.05$ produced a planar surface. Further path enlargement and the addition of a peripheral cut-off wall maintained surface planarity but increased material loss. However, the cut-off wall clearly separated retained from lost sand, enabling maintenance of a constant fall height. In a separate test series, vertical homogeneity was evaluated using unwashed KS, filling a mold composed of four stacked rings and calculating the mean dry density of the sand in each ring. The two repeated tests produced consistent ring averaged dry densities over the specimen height and the bottom ring was systematically looser. Overall, the results demonstrate that RASP can be transferred to large cylindrical specimens, provided that the trajectory coverage is adapted to the effective sand rain footprint and that boundary induced effects are considered.

1 Introduction

Laboratory tests on granular soils are commonly interpreted as element tests, although the initial state of a reconstituted specimen depends on mean density, spatial density variation, depositional fabric and boundary conditions. Preparation induced differences can change stiffness, dilatancy, strength and localization. Arthur and Phillips [1] demonstrated that

* Corresponding author: carlos.pinto@kit.edu

inherent anisotropy and loose layer geometry affect specimen deformation, whereas Miura and Toki [3] showed that preparation method influences dilatancy and anisotropic fabric. Consequently, mean dry density alone is not a sufficient quality descriptor.

Dry air pluviation can typically achieve mean relative densities of approximately 0.2 to 1.0 without mechanical compaction; however, manual nozzle motion, fall height variations and interruptions can reduce reproducibility. Robotic automated specimen preparation (RASP) replaces manual movement by a programmable robot and records the three-dimensional nozzle trajectory. Using RASP, Mugele et al. [2] prepared more than 80 specimens, which showed lower density variability than manually prepared specimens. Their study further demonstrated that nozzle diameter and fall height had clear effects on the achieved density, whereas nozzle velocity and path pattern had comparatively minor effects within the investigated ranges. In addition, they identified a systematically looser bottom layer, which was attributed to grain impact and rebound at the initially rigid base.

Large-scale triaxial testing is required when standard specimens cannot represent coarse field materials. In tests on alluvial gravel specimens with diameters of 100, 150 and 800 mm, Girumugisha et al. [6] observed markedly lower dilatancy and slightly higher stiffness and peak strength at the larger scale, mainly because scaling altered grading and packing. Mugele et al. [5] further showed that preparation induced fabric can influence the undrained behavior of sand even at comparable density and stress. These findings motivate a reproducible method for preparing large specimens; the present study addresses this prerequisite but does not itself quantify mechanical specimen size effects.

Building on the preparation parameters investigated by Celler [4], the present scale-up initially focused on dense specimens, which provided a reproducible starting condition for transferring RASP to larger dimensions. However, when the method was scaled to diameters approaching 500 mm, a new problem emerged: the deposited surface became systematically higher near the center. This central crown prevented full, planar contact with a subsequent loading plate and raised the question of whether the specimen was deposited homogeneously across the specimen radius. In parallel, the study examined whether the ring averaged dry density remained uniform and reproducible over the specimen height after scaling the pluviation path. The broader aim was to establish a first step for reliable preparation procedure for specimens intended for large-scale geotechnical element tests, including triaxial and oedometer tests.

The experimental program therefore comprised two complementary but separate test series. The first documented the center high deposition surface and subsequently investigated the effects of path diameter, path topology and the peripheral boundary. The second examined the vertical distribution of ring averaged dry density using a stacked ring mold. Together, the series addressed whether the layer averaged dry density remained uniform and reproducible over the specimen height and which tested trajectory provided a planar surface with acceptable material loss.

2 Experimental program

2.1 Material and RASP system

Karlsruhe Sand (KS) was used, with d_{10} = 0.40 mm, d_{50} = 0.55 mm, d_{90} = 0.90 mm and particle density ρ_s = 2.65 g/cm³ [2]. KS were used in two forms: unwashed KS, in which the fine fraction ($d < 0.063$ mm) present in the as-delivered material was retained and washed KS, from which this fine fraction was removed by washing. For the unwashed material, the minimum and maximum dry densities determined in the laboratory were $\rho_{d,min}$ = 1.423 g/cm³

and $\rho_{d,max}$ = 1.668 g/cm^3, respectively. The corresponding values for washed KS were 1.420 and 1.692 g/cm^3 [4].
The RASP system comprised a six-axis collaborative robot (cobot, see Fig. 1 a)) carrying a hopper fitted with a nozzle and sand was deposited in successive layers following either serpentine or concentric paths. The spacing between adjacent tracks (l_s) was maintained at 5 mm. To avoid systematic superposition of the deposition paths, the trajectory of each successive layer was rotated by 17 clockwise. After each layer, the nozzle was raised by a height increment of Δh to maintain the prescribed fall height h_f [2].

$$\Delta h = 4\dot{m} \cdot \Delta t \,/\, (\rho_{d,t} \cdot \pi D^2) \quad (1)$$

where $\dot{m}$ is the calibrated mass flow rate, Δt is the effective deposition time per layer, D is the internal diameter of the mold and $\rho_{d,t}$ is the target dry density. Mass flow rates of 1.59 g/s and 1.51 g/s for a 4 mm nozzle diameter were measured for unwashed and washed KS, respectively. As also reported by Celler [4] the mass flow rate must be calibrated for the actual material and hopper-nozzle system.

Based on the preparation parameters previously established for dense KS specimens [4], all experiments reported here were conducted using a nozzle diameter of 4 mm and a prescribed fall height of 270 mm. Furthermore, during the experimental program, a gravity fed reservoir with a capacity of approximately 17 L, located at a height of 600 mm from the hopper top, was adapted to the system to reduce interruptions caused by refilling the hopper.

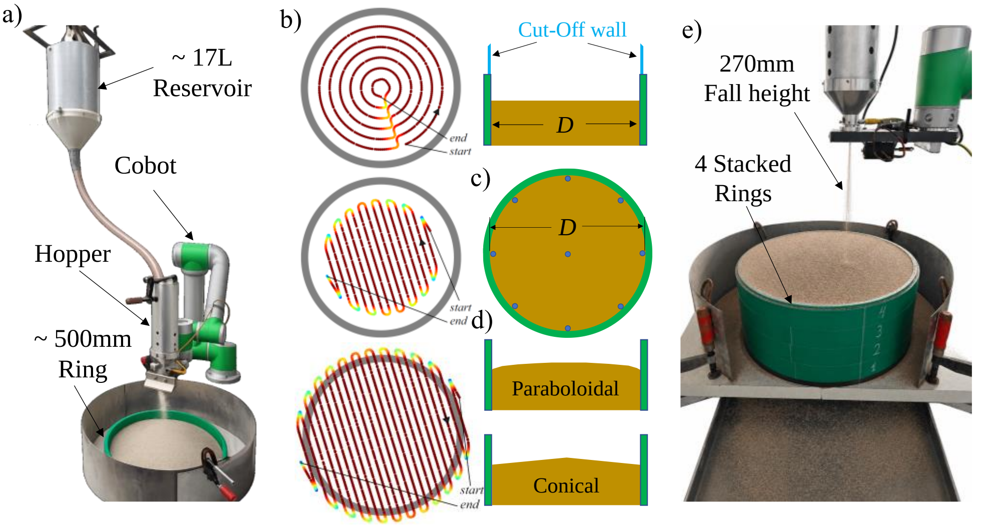

Fig. 1. a) Large-scale RASP configuration; b) plan view of the nozzle path topologies (concentric, serpentine and enlarged serpentine) from [2] and diametral section of the peripheral cut-off wall boundary condition; c) plan view of the single-ring cylindrical mold with measuring points; d) equivalent volume representation using paraboloidal and conical approximations of the central crown in a single-ring cylindrical mold; and e) stacked rings configuration used to assess vertical density uniformity.

2.2 Surface geometry, loss and equivalent specimen volume

Seven tests were conducted with washed KS in a single-ring cylindrical mold of nominal internal diameter D = 469.4 mm and ring height h_r = 50 mm, using a calibrated mass flow rate of 1.51 g/s and a fall height of h_f = 270 mm. The path diameter, path topology and peripheral boundary condition were varied to investigate the formation and reduction of the center high deposition surface. For example, in one test, a thin 20 mm high peripheral cut-off wall with a sharp upper edge was installed vertically along the inner perimeter of the mold (see Fig. 1 b)). For each test, the final upper surface of the sand deposited within the mold was surveyed at eight equally spaced points along the perimeter and at one point at the center (see Fig. 1 a) and c)). The surface depth d was measured vertically downwards from a fixed reference level. The central rise (Δz_c), defined relative to the mean perimeter elevation, was calculated as:

$$\Delta z_c = \bar{d}_{edge} - d_c \quad (2)$$

where $\bar{d}_{edge}$ is the mean depth measured at the eight perimeter points and d_c is the depth measured at the center. In addition to the surface survey, the mass retained inside the mold (m_{in}) and the mass deposited outside it (m_{loss}) were recorded. Accordingly, the proportion of the total pluviated material lost outside the mold was calculated as:

$$\lambda_m\ (\%) = [m_{loss} / (m_{in} + m_{loss})] \cdot 100\% \quad (3)$$

Because these specimens were not levelled after pluviation, their retained volume could not be represented by a cylinder with a planar upper surface. Therefore, an equivalent volume was estimated as the sum of the cylindrical volume extending from the specimen base to the mean perimeter height ($\bar{H}_{edge}$) and an idealized axisymmetric correction for the central rise:

$$V_{eq} = A \cdot [\bar{H}_{edge} + \alpha\ (\bar{d}_{edge} - d_c)] \quad (4)$$

$$V_{eq} = A \cdot [H_{ref} - \bar{d}_{edge} + \alpha\ (\bar{d}_{edge} - d_c)] \quad (5)$$

where $A = \pi D^2/4$, H_{ref} is the vertical distance from the specimen base to the reference level, and α represents the assumed crown geometry. A conical crown corresponds to α = 1/3, whereas a paraboloidal crown corresponds to α = 1/2 (see Fig. 1 d)). The normalized central rise, Δz_c / $\bar{H}_{edge}$, and the equivalent mean dry density, $\rho_{d,eq} = m_{in}/V_{eq}$., were subsequently calculated.

To express the calculated equivalent density relative to the limiting states determined in the laboratory, the equivalent relative density was calculated as:

$$I_{D,eq} = (1/\rho_{d,min} - 1/\rho_{d,eq}) / (1/\rho_{d,min} - 1/\rho_{d,max}) \cdot 100\% \quad (6)$$

Finally, to investigate whether the center high surface also developed at a smaller specimen scale, two additional tests were conducted in a cylindrical mold with a diameter of D = 295 mm. The same surface survey and evaluation procedures were applied. Within this test pair, only the path diameter was varied, allowing the magnitude of the central rise to be compared between the two mold sizes.

2.3 Vertical density tests

Two replicate specimens of unwashed KS were prepared in a mold comprising four stacked rings with a nominal internal diameter D = 469.4 mm, an individual ring height h_r = 50 mm and a total height H = 200 mm (see Fig. 1 e)). The calibrated mass flow rate was 1.59 g/s, the path diameter D_p = 449.4 mm and the fall height h_f = 270 mm. After overfilling and levelling the specimen at the upper rim, the rings were separated successively from the top. The material in each ring was then levelled at the corresponding ring edge and weighed. The dry density of ring i was calculated as:

$$\rho_{d,i} = 4 \cdot m_{d,i} / (\pi \cdot D_i^2 \cdot h_r) \quad (7)$$

where $m_{d,i}$ and D_i are the dry mass and internal diameter of ring i, respectively.

To express the achieved density relative to the limiting states determined in the laboratory, the relative density was calculated as:

$$I_{D,i} = (1/\rho_{d,min} - 1/\rho_{d,i}) / (1/\rho_{d,min} - 1/\rho_{d,max}) \cdot 100\% \quad (8)$$

The vertical uniformity within each specimen was assessed using the coefficient of variation (CV) of the ring averaged dry densities:

$$CV_x = (s_x / \bar{x}) \cdot 100\% \quad (9)$$

Where s_x and $\bar{x}$ are the sample standard deviation and mean of variable x, respectively. For the statistical analysis, the bottom ring was excluded to prevent its boundary associated deviation from disproportionately influencing the assessment of the upper rings.

3 Results

A feature common to all tests was the widening of the sand stream during free fall. With the selected nozzle diameter of 4 mm and fall height of 270 mm, the stream had an approximate footprint diameter of 20 mm upon reaching the deposition surface.

3.1 Surface geometry, boundary interaction and sand capture

Table 1 and Fig. 2 summarize the test program for the large (L) and small (S) specimens and reveals three main trends. First, trajectories terminating at or within the mold internal diameter (D_p / $D \leq 1$) produced a center high surface ($\Delta z_c > 0$), irrespective of whether a serpentine or concentric path was used. Second, extending the serpentine path beyond the mold internal diameter (D_p / $D > 1$) produced a planar surface ($\Delta z_c = 0$), although further increasing the path diameter resulted in greater material loss. Third, introducing a peripheral cut-off wall maintained surface planarity and provided a clearly defined boundary between retained and lost sand, but increased material loss relative to the corresponding open rim (without cut-off wall) configuration. The two smaller diameter tests are considered exploratory and are not treated as a matched scaling series because only the path diameter was varied and the broader test sequence was not replicated at this scale.

Table 1. Surface geometry conditions, sand loss and equivalent total dry density.

Test	D (mm)	D_p (mm)	Boundary	Path	Reservoir	Δz_c (mm)	$\frac{\Delta z_c}{\bar{H}_{edge}}$ (%)	λ_m (%)	$\rho_{d,eq}$ (g/cm^3) Paraboloidal - Conical	$I_{D,eq}$ (%) Paraboloidal - Conical
L8	469.4	449.4	Open rim	Concentric	Active	4.6	11.7	0.3	1.71 - 1.75	106.8 - 116.4
L2	*469.4*	*449.4*	*Open rim*	*Serpentine*	*No*	*7.8*	*18.1*	*0.6*	*1.67 - 1.72*	*93.1 - 107.7*
L5	*469.4*	*449.4*	*Open rim*	*Serpentine*	*Active*	*6.0*	*14.8*	*0.6*	*1.69 - 1.73*	*98.3 - 110.4*
L3	*469.4*	*469.4*	*Open rim*	*Serpentine*	*No*	*4.3*	*10.2*	*2.3*	*1.68 - 1.70*	*94.7 - 103.2*
L6	*469.4*	*489.4*	*Open rim*	*Serpentine*	*Active*	*0.0*	*0.0*	*7.0*	*1.69*	*99.5*
L7	*469.4*	*509.4*	*Open rim*	*Serpentine*	*Active*	*0.0*	*0.0*	*12.6*	*1.72*	*108.1*
L9	*469.4*	*489.4*	*20 mm peripheral cut-off wall*	*Serpentine*	*Active*	*0.0*	*0.0*	*9.7*	*1.67*	*93.2*
S2	295.0	275.0	Open rim	Serpentine	Active	5.0	8.7	0.7	1.66 - 1.68	90.0 - 97.4
S1	295.0	295.0	Open rim	Serpentine	Active	1.5	2.3	3.7	1.66 - 1.67	90.5 - 92.5

The dry density and relative density ranges reported in Table 1 are global volume reconstructions and do not represent measurements of radial density variation. The width of each range reflects the unknown radial shape of the upper surface between the measured center and perimeter elevations. For the same center rise, the assumed paraboloidal profile gives a larger specimen volume (and hence a lower equivalent dry density) than the conical profile. Several of the upper estimates exceed the reference maximum dry density and some tests show relatively wide ranges between the two geometric assumptions. These values should therefore be regarded as model dependent approximations rather than precisely constrained density bounds. The available surface survey is insufficient to determine the actual radial profile and, consequently, the specimen volume with the required accuracy. Nevertheless, the estimates provide an indicative reference showing that the adopted pluviation procedure consistently produced very dense specimens, with $I_D > 90\%$.

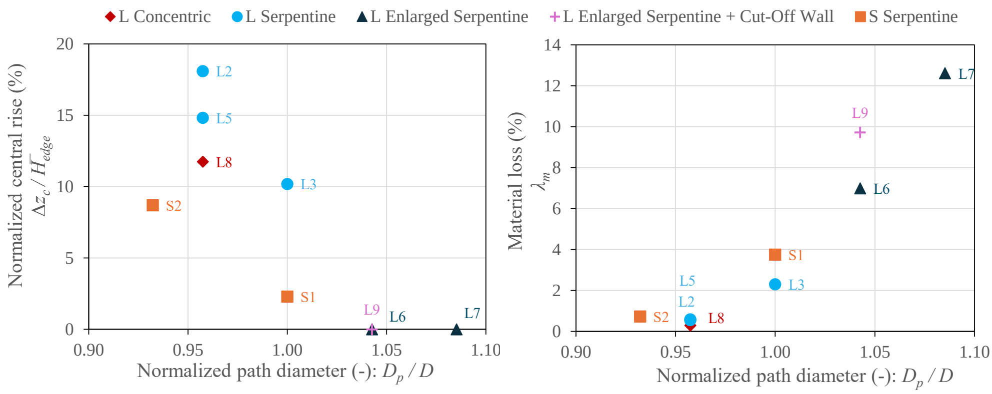

Fig. 2. Normalized central rise and material loss versus normalized path diameter. Enlarged L6, L7 and L9 produced planar surface surveys; among these configurations, L6 had the lowest material loss.

3.2 Vertical density uniformity

Following the procedure described by Mugele et al. [2], a target dry density of 1.69 g/cm^3 was adopted for unwashed KS based on the selected nozzle diameter and fall height. This value exceeded the laboratory reference maximum dry density of 1.668 g/cm^3 and several measured ring densities also exceeded this reference value; consequently, relative densities shown in Fig. 3 are greater than 100%.

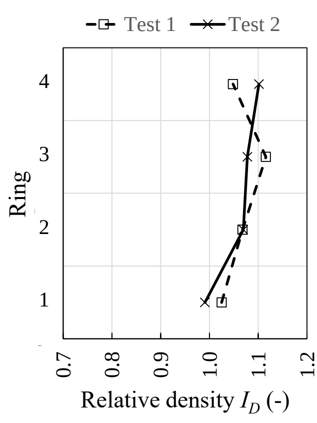

Ring / Statistic	Test 1 Dry density $\rho_{d,i}$ (g/cm^3)	Test 1 Relative density $I_{D,i}$ (%)	Test 2 Dry density $\rho_{d,i}$ (g/cm^3)	Test 2 Relative density $I_{D,i}$ (%)
4 (top)	1.68	104.8	1.70	110.3
3	1.70	111.6	1.69	107.9
2	1.69	106.9	1.69	106.9
1 (bottom)	1.68	102.4	1.67	99.0
Mean, rings 2–4	1.69	*107.8*	1.69	*108.3*
CV, rings 2–4 (%)	0.6	*3.2*	0.3	*1.6*

Fig. 3. Vertical dry density and relative density profiles for the two stacked rings specimens. Statistics were calculated using Rings 2 - 4 (bottom ring was excluded).

Under the selected pluviation conditions, the two replicate specimens achieved nearly identical mean dry densities (see Fig. 3): Excluding the consistently looser bottom ring, only small deviations from the respective mean were observed among the three statistically evaluated upper rings (Rings 2 - 4).

4 Discussion

4.1 Path coverage and surface planarity

For the selected enlarged path, the outermost nozzle centerline extended 10 mm beyond the mold internal diameter, corresponding to approximately half the observed impact-footprint width. Consequently, part of the broadened deposition footprint covered the perimeter instead of terminating wholly inside the opening. This configuration produced a planar surface survey in the tested configuration. However, this observation represents an empirical coverage rule, not a universal scaling law: the footprint should be remeasured when the nozzle, sand or fall height changes. Additionally, this boundary coverage consideration becomes particularly relevant when transferring RASP from conventional specimens of approximately 100 mm in diameter to larger specimens, for which paths defined solely by the mold internal diameter may not produce a planar surface.

The concentric trial shows that changing the path topology alone did not eliminate the central rise when the path remained inset. Furthermore, although both the open rim and cut-off-wall configurations produced a planar surface, they imposed different boundary conditions. The open rim resulted in lower measured material loss; however, the amount of sand crossing or rebounding back into the mold could not be controlled or quantified reliably, thereby introducing uncertainty into the retained mass and the resulting layer height increment. By contrast, the cut-off wall provided a clearly defined boundary between retained and lost material. Among the tested configurations, the enlarged serpentine path combined with the cut-off wall therefore provided the best balance between surface planarity, controlled material retention and reliable determination of the nozzle height increment (Δh), required to maintain a constant fall height. This conclusion should nevertheless be confirmed through denser surface mapping, local density measurements and direct monitoring of the actual layer height development.

4.2 Interpretation of vertical density uniformity

The stacked rings tests demonstrate repeatable layer averaged dry densities within the established portion of the specimen. However, because each ring was weighed as a single volume, the results do not demonstrate radial or circumferential density homogeneity. Both specimens showed a reproducible lower value in the bottom ring. Although this trend is consistent with the grain impact and rebound mechanism reported by Mugele et al. [2], it cannot be attributed directly to the rigid base based on the present measurements. Owing to the greater ring height used in this study, any near base rebound affected zone may have constituted a smaller proportion of the bottom ring volume than in the experiments of Mugele et al. [2]. Consequently, the measured bottom ring density represents an average over the entire 50 mm thick layer and does not resolve either the thickness or the local density of a potentially looser near base zone.

4.3 Scope and limitations

The experimental program followed sequential optimization rather than a fully crossed design. The reservoir configuration changed during the program, the stacked ring validation used unwashed KS whereas the surface path trials used washed KS, and the complete large ring sequence was not replicated in the small mold. In addition, the surface survey sampled only the center and perimeter, leaving the intermediate radial profile unresolved. Consequently, comparisons involving reservoir state, material condition or mold diameter may be confounded. The results support vertical layer mean repeatability and configuration specific path optimization, but they do not establish a diameter dependent scaling law, complete radial or circumferential density homogeneity, or a mechanical specimen size effect.

5 Conclusions

The large stacked ring specimens reproduced a comparably dense and vertically uniform state. Nevertheless, the bottom ring was consistently looser; although this trend is compatible with the near base impact and rebound mechanism reported in the literature, the 50 mm layer averages do not identify its cause or local extent. Regarding surface geometry, a center high surface developed whenever the trajectory terminated at or within the mold internal diameter and changing from a serpentine to a concentric trajectory did not eliminate it. By contrast, extending the serpentine path 10 mm beyond the mold internal diameter produced a planar surface. Both the open rim and cut-off wall configurations maintained surface planarity, however, the cut-off wall provided a clearly defined boundary between retained and lost sand, enabling the maintenance of a constant fall height.

Accordingly, the required path extension should not be regarded as a universally applicable value but should be selected for each configuration based on the measured footprint of the sand stream at the deposition surface. Furthermore, the integration of a gravity fed reservoir with a capacity of approximately 17 L reduced refill interruptions and facilitated the automated preparation of large specimens. Overall, the results demonstrate reproducible control of layer averaged dry density above the bottom ring and provide a practical basis for optimizing deposition path coverage to achieve a planar surface. They do not, however, demonstrate radial density homogeneity, establish a diameter dependent scaling law or quantify a mechanical specimen size effect.

References

1. J.R.F. Arthur, A.B. Phillips, Homogeneous and layered sand in triaxial compression. Géotechnique 25, 799-815 (1975). doi:10.1680/geot.1975.25.4.799
2. L. Mugele, J.D. Arroyo Lopez, J. Zürn, H.H. Stutz, Robotic automated specimen preparation (RASP): applied to air pluviation. Acta Geotech. (2026). doi:10.1007/s11440-026-03112-4
3. S. Miura, S. Toki, A sample preparation method and its effect on static and cyclic deformation-strength properties of sand. Soils Found. 22, 61-77 (1982). doi:10.3208/sandf1972.22.61
4. L. Celler, Bachelorarbeit, Untersuchungen zum Einfluss der Homogenität von Bodenproben auf die resultierenden bodenmechanischen Versuchsergebnisse Institute of Soil Mechanics and Rock Mechanics, Karlsruhe Institute of Technology (2026).
5. L. Mugele, J. Zürn, A. Niemunis, H.H. Stutz, Experimental study of the soil structure variable z used in constitutive models such as Neohypoplasticity or Sanisand. IOP Conf. Ser.: Earth Environ. Sci. 1480, 012070 (2025). doi:10.1088/1755-1315/1480/1/012070
6. G. Girumugisha, C. Ovalle, H. Reith, H.H. Stutz, Effects of triaxial sample scaling on the mechanical behavior of alluvial gravels. J. Geotech. Geoenviron. Eng. 152(1), 04025166 (2026). doi:10.1061/JGGEFK.GTENG-13923